ISSN 0023-1584, Kinetics and Catalysis, 2018, Vol. 59, No. 4, pp. 418–427. © Pleiades Publishing, Ltd., 2018.

Heterostructured MgO/ZnO photocatalysts: Synthesis, Characterization and UV Light-Induced Photocatalytic Activity Using Model Pollutant 2,6-dichlorophenol[1]

A. I. Vaizogullar*

Medical Services and Techniques Department, Vocational School of Health Services, Muğla Sıtkı Koçman University, Muğla, Menteşe, 48000 Turkey

**e-mail: aliimran@mu.edu.tr*

Received May 11, 2017; in final form, December 21, 2017

Abstract—ZnO and MgO/ZnO (mass ratio 2 : 5, 5 : 5 and 8 : 5) heterostructure photocatalysts (Mg_2Zn_5, Mg_5Zn_5 and Mg_8Zn_5, respectively) were successfully synthesized via co-precipitation method. MgO/ZnO composites were characterized by scanning electron microscopy (SEM), X-Ray diffraction and low temperature nitrogen adsorption–desorption isotherm. According to SEM images all composites consisted of spherical granules with particle sizes of 30–50 nm. The band gap value of ZnO was found to be lower than that of MgO/ZnO composites as observed during the optical studies. Pure ZnO showed lower photocatalytic activity (38%) in the degradation of 2,6-dichlorophenol (2,6-DCP) than MgO/ZnO composites. Mg_5Zn_5 composite with a higher concentration of defects in crystallites was more active in the photocatalytic degradation (79.5%) than Mg_8Zn_5 (61.2%) and Mg_2Zn_5 (63.5%). High-resolution mass spectrometry-and UV-Vis spectroscopic analysis of the by-products, derived from model pollutant 2,6-DCP, proved the successful photocatalytic performance of Mg_5Zn_5 under the UV light. The synthesized composites are future candidates against other potential environmental pollutants.

Keywords: phenol, advanced oxidation, chloro-organic pollutants, photodegradation, MgO/ZnO photocatalyst

DOI: 10.1134/S0023158418040146

Industries are becoming the backbone of economies as well as a job market. Together with their benefits, they also carry drawbacks. One of the most important problems associated with the industrial development is the sewerage wastewater. Although it should be treated and then released into the environment, very few countries perform this practice due the cost or complications in the procedures.

There are various useful processes to treat wastewater such as adsorption, membrane systems and electrocoagulation. These processes are either expensive or painstaking. In this regard, semiconductor catalysts are most suitable, popular and cheap as they utilize sunlight as renewable energy [1]. As an example, ZnO, a photocatalyst, has been reported as non-toxic, highly photosensitive, possessing strong oxidizing power and photochemical stability [2, 3]. Pure ZnO has a large band gap energy i.e. 3.2 eV. In the presence of UV/visible light, the electrons in ZnO are excited from the valence band to the conduction band. The subsequent drift of electron-hole pairs from the ZnO surface after this excitation initiates the photocatalytic reaction. The lower separation rate of electron-hole pairs reduces photocatalytic reaction yield. This problem can be tackled using coupled structure semiconductors. This definition addresses two different semiconductors present together in a photocatalytic system as hetero-junctions to show enhanced photocatalytic activity [4].

ZnO can be used in combination with different metal oxides i.e. MgO, CuO, Fe_2O_3 etc. Mg-doped Zn semiconductors have shown surprising results. Kulubnuan et al. [5] have synthesized MgO/ZnO nanocomposites by a hydrothermal method and found that photocatalytic degradation is inversely proportional to the amount of MgO. Zhao and coworkers [6] have reported morphological structure of MgO/ZnO as nanosheetts where MgO caused zigzag edges with angles of 120° in the MgO/ZnO system. Al-Naser et al. [7] have synthesized $Zn_{1-x}Mg_xO$ (x = 0, 2 and 5%) microtubes via microwave heating method. They emphasized that UV-Vis absorption peak related to ZnO showed blue shift from λ_{max} = 379 (3.27 eV) to 370 nm (3.35 eV) for $Zn_{0.95}Mg_{0.05}O$ microtubes when

[1] The article is published in the original.

MgO content was increased. Bobu and coworkers [8] observed hyperchromic shift in UV and green emission when MgO content was decreased. Suwanboon et al. [9] have synthesized composite $Zn_{1-x}Mg_xO$ nanostructures by the sol–gel method. They found a decrease in crystal size when Mg content was increased to $x = 0.05$. The prepared $Zn_{0.95}Mg_{0.05}O$ catalyst exhibited higher efficiency in the degradation of methylene blue.

The results outlined above suggest that a proportional increase of MgO does not improve catalytic and optical properties of ZnO. In this study, we have introduced different amounts of MgO into ZnO to obtain MgO/ZnO nanocomposites by co-precipitation method using N-propylamine as stabilizer. Herein, we also report the optical, structural and photocatalytic properties of MgO/ZnO composites in the degradation of 2,6-dichlorophenol (2,6-DCP).

EXPERIMENTAL

Preparation of ZnO and MgO/ZnO Nanocomposites

Pure ZnO particles were synthesized by chemical precipitation method. To prepare solution A, 64 g (0.296 mol) of $Zn(Ac)_2 \cdot 2H_2O$ (≥97%, Merck) was dissolved in 200 mL of distilled water. Then, to solution A 53 mL of 0.1 M NH_4OH solution (97%, Carlo Erba) was dropped and stirred for 4 h. The reaction mixture was filtered and washed with distilled water, dried at 80°C for 4 h and calcined at 600°C for 3 h.

A series of MgO/ZnO composites with various MgO content was prepared by co-precipitation method. To prepare solution A, 0.062 mol of $Zn(Ac)_2 \cdot 2H_2O$ (Sigma-Aldrich) was dissolved in water/*n*-propylamine (100 mL) solutions (4 : 1, *v*/*v*) and stirred at 45°C for 30 min. Stoichiometric amounts (30, 50, 60 wt %) of $Mg(NO_3)_2 \cdot 6H_2O$ were added to solution A with stirring to synthesize MgO/ZnO composite catalyst. Then, to the mixture 0.1 M of ammonia hydroxide (65 mL) (Merck) was dropped and stirred at 45°C for 4 h. Solid particles thus obtained were filtered and washed thrice with distilled water. The samples were dried at 80°C in an oven and calcined at 600°C for 4 h. The synthesized MgO/ZnO composites were denoted as Mg_2Zn_5, Mg_5Zn_5 and Mg_8Zn_5 where the subscripts signify the weight amounts of MgO and ZnO in the composites.

Characterization and Photocatalytic Activity Measurements

The crystalline structure was examined by XRD (Dmax 350, Rigaku, Japan) using CuK_α radiation (λ = 0.154056 nm). The microstructure and shape of the particles were investigated using a scanning electron microscope (SEM) (JSM-7600F, JEOL, Japan). Elemental composition was determined using an EDAX analyzer (JSM-7600F). BET surface area, pore volume, and pore size were measured using a ASAP 2010 (Micromeritics Instrument, USA) with N_2 adsorption at 77.35 K.

A specially designed UV reactor was used in the photolytic experiments with five UV light sources (254 nm, 20 W) at ambient temperature and atmospheric pressure. In addition to the photocatalytic kinetics experiments, 2,6-dichlorophenol (2,6-DCP) decomposition intermediates were also evaluated using UV-visible spectroscopy and high-resolution mass spectrometry (HRMS) at different intervals of degradation procedure. HRMS analyses were carried out using a SYNAPT G1 MS system (Waters Corp., USA) with experimental conditions as follows: sampling cone 30 V, extraction cone 4 V, source temperature 80°C, desolvation temperature 250°C and capillary voltage 2 kV.

RESULTS AND DISCUSSION

SEM Analyses

SEM analyses (Fig. 1) were carried out to study the morphology of the prepared catalysts. Morphological features were nearly the same for all samples. The images of pure ZnO and all composites show aggregates of smaller particles. The aggregation density of the composites was increased with increasing MgO content. It is expected that coarsening can negatively affect the photocatalytic activity of the composites in the degradation of organic pollutants. SEM results are consistent with results of XRD measurements (Fig. 2). In addition, the size of secondary particles of pure ZnO, Mg_2Zn_5 and Mg_5Zn_5 was about 100 nm while in was 50 nm in the case of Mg_8Zn_5.

Figure 2 shows XRD pattern of the prepared composites. In all patterns, the wurtzite structure of hexagonal ZnO can be recognized as the main phase (JPDS 36-1451). In addition, the peak at $2\theta = 42.8°$ due to MgO is clearly seen in the MgO/ZnO samples (JPDS-89-7746) indicating the formation of the composites. Generally, the peak intensity of MgO increases with increasing amount of MgO. On the contrary, the peak height of ZnO decreases with concomitant broadening as evidenced by the XRD patterns of Mg_5Zn_5 catalysis. A possible explanation might be that MgO is well dispersed onto ZnO surface. Broadening of ZnO peaks indicates that Mg_5Zn_5 particles have a smaller size as compared to other samples. Higher density of crystalline defects in Mg_5Zn_5 catalyst has already been reported [10].

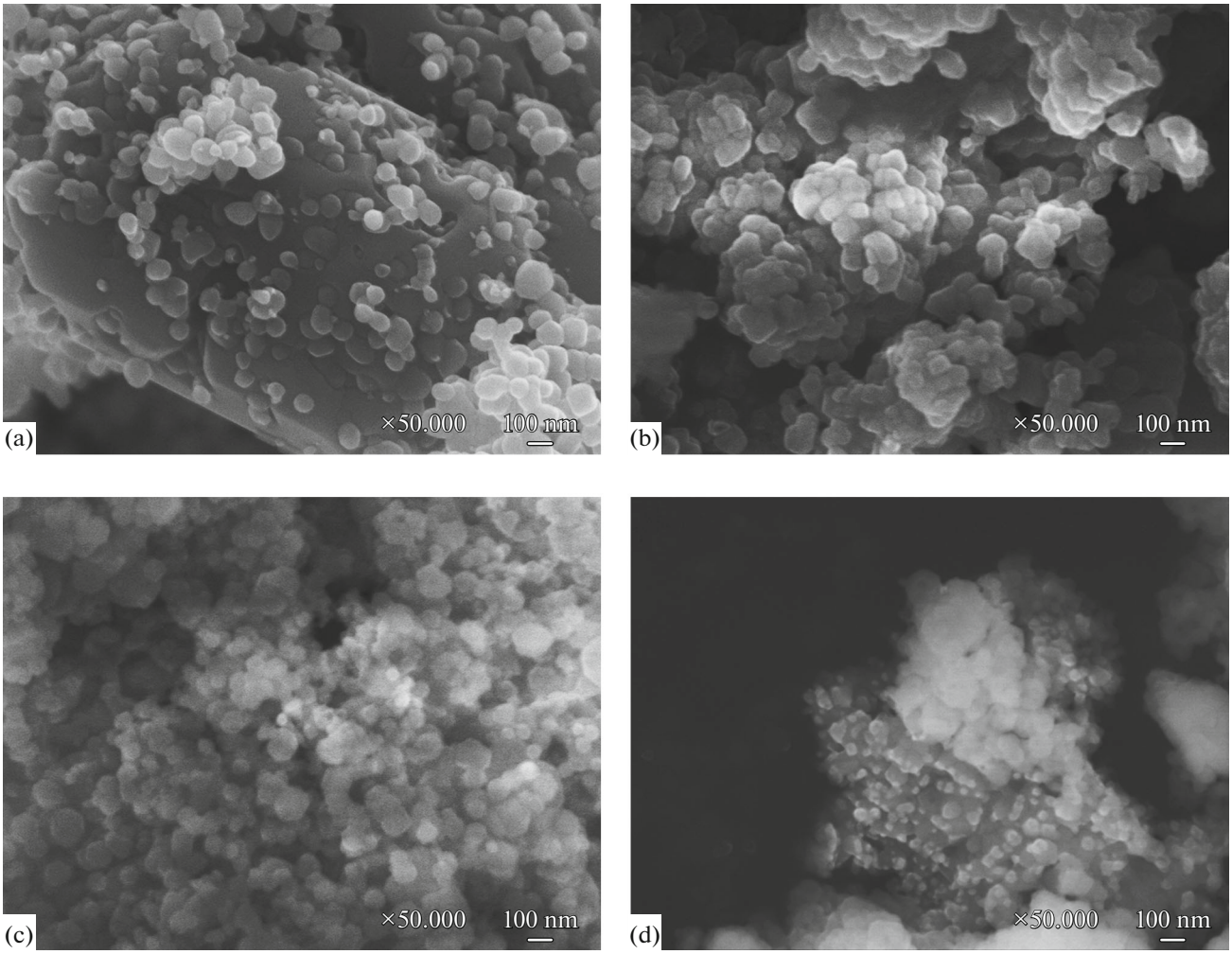

Fig. 1. SEM images of ZnO (a), Mg_2Zn_5 (b), Mg_5Zn_5 (c) and Mg_8Zn_5 (d) composites.

The crystal sizes of the prepared catalysts were calculated (Table 1) using Scherrer equation (eq. 1).

$$d = \frac{B\lambda}{\beta_{1/2}\cos\theta}, \quad (1)$$

where d is the average particle size, B is the Scherrer constant (0.94), λ is the wavelength of the X-Ray, $\beta_{1/2}$ is full width at half maximum of the diffraction peak and θ is the diffraction angle. Pure ZnO particles showed larger crystallite sizes due to higher crystallinity (Table 1). In addition, it appears that the crystal size initially decreased and then increased as a function of MgO content.

The differences in crystal sizes may be due to two reasons. First, the particle radius of Mg^{2+} is similar with the bulk ZnO exciton Bohr radius, so, quantum confinement effects can be expected [11]. Second, Zener pinning effect can be considered [5]. The crystal size of composites may be affected by changing the MgO content. The strong ZnO peaks (Fig. 2) shows that the ZnO particles are well crystallized by the thermal annealing at 600°C [12]. Estimated error for ZnO and MgO in the XRD results for its characteristic peaks was obtained below 36° (2θ degree). The observed shifts in the XRD results confirm the presence of crystallite defects in the composite structure.

Now we can discuss the effect of stress on the crystallite size. The magnitude of stress can be calculated using below equation 2 [13] with the values tabulated in Table 1.

$$\sigma = \frac{-233\times10^9\left(C_{\text{Sample}} - C_{\text{Bulk}}\right)}{C_{\text{Bulk}}}, \quad (2)$$

where C_{sample} is the lattice constant of ZnO and C_{bulk} is the strain free lattice constant of ZnO (5.206 Å). Stress undergoes transformation from a positive tensile to a negative compressive form that would lead to decline in the crystal size. It is possible that the stress prevents the growth of composite particles [13].

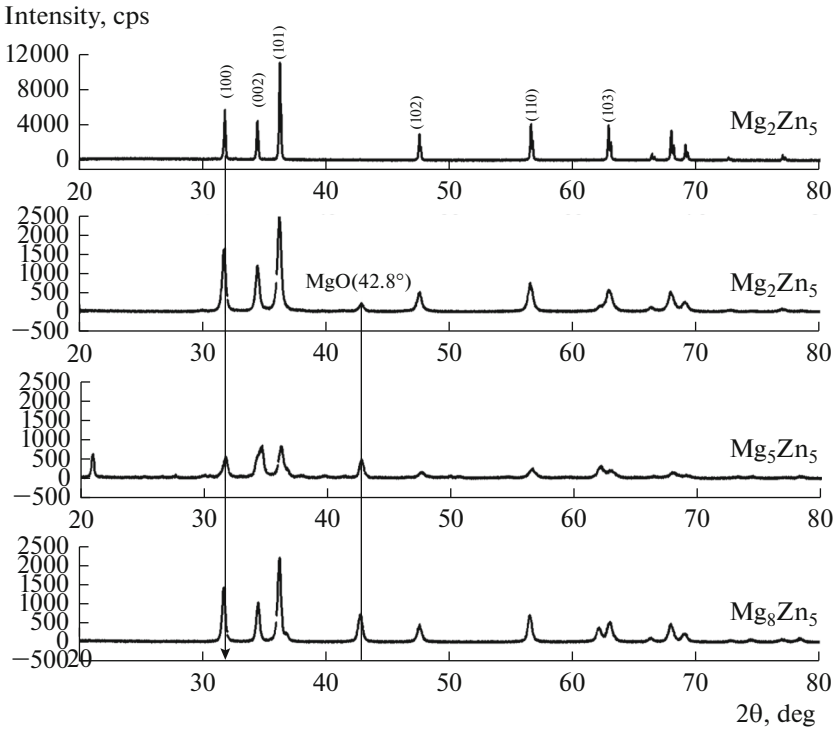

Fig. 2. XRD results of ZnO and MgO/ZnO composites.

Optical Properties

The effect of MgO content on the band gap value was also investigated (Fig. 3). Each sample has a high absorbance around 300–400 nm. The optical band gap value was determined using $E_g = \frac{1240}{\lambda}$ equation, where λ is the onset to the rising part to the *x*-axis of the plots shown by the dotted line. The obtained E_g value of each sample is higher than that of ZnO (3.44 eV) (Table 1). MgO/ZnO composites possess ordered structure and have fewer defects than ZnO. E_g values of Mg_2Zn_5, Mg_5Zn_5 and Mg_8Zn_5 composites were found to be 3.54, 3.49 and 3.58 eV, respectively (Fig. 3, inset). These values reflect the presence of both metal oxides; and MgO presence causes a blue shift [14], especially pronounced at higher amounts of MgO. Increased amounts of MgO slightly increase the separation between defect levels. This situation leads to a blue shift in emission for ZnO that possibly originates from the Zn_i (interstitial) defect [15]. The above discussion supports the conceptual premise that a lower E_g value of Mg_5Zn_5 catalyst within the MgO/ZnO composites indicates an increased population of crystalline defects in the Mg_5Zn_5 composite [16].

Photoluminescence Analysis (PL)

Photoluminescence spectra of the ZnO and MgO/ZnO composites with excite on emission at 300 nm are presented in Fig. 4. The PL spectrum of the ZnO shows a sharp UV emission peak at 384 nm due to extinction of excitons [17]. Also, blue-green emission

Table 1. The physical properties and kinetic results of each sample

Catalyst	d_{MgO}, nm	d_{ZnO}, nm	Lattice constant *c*, Å	σ, 10^9 Pa	E_g, eV	BET, m^2/g	$k \times 10^{-3}$, min^{-1}
ZnO	–	33.6	5.205	0.044	3.40	3.6	4.8
Mg_2Zn_5	25.5	26.9	5.198	0.358	3.54	74	8.7
Mg_5Zn_5	24.2	16.1	5.216	–0.447	3.49	57	14.2
Mg_8Zn_5	26.1	30.4	5.192	0.357	3.58	67	5.1

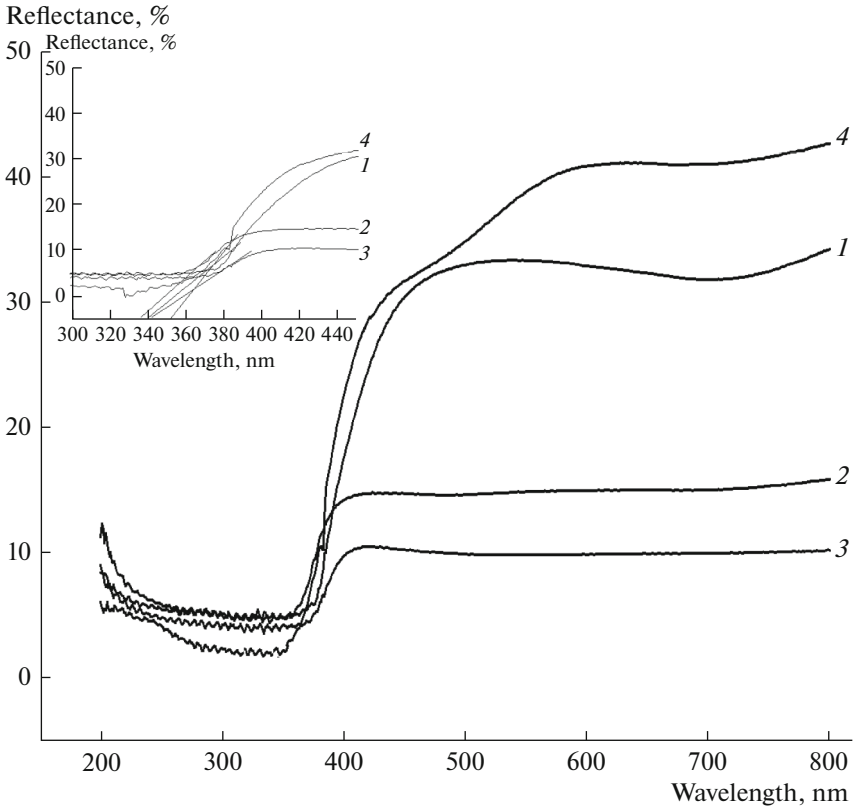

Fig. 3. UV-DRS spectra of ZnO (*1*) and MgO/ZnO composites: (*2*) Mg_5Zn_5, (*3*) Mg_5Zn_5, (*4*) Mg_2Zn_5.

bands at 421, 460 and 484 nm are present in the spectrum. The green emission band at 531 nm indicates impurities in structure such as Zn interstitials (Zn_i) and oxygen vacancy (O_v) [18]. The PL spectrum of the MgO/ZnO samples contains UV and visible emission peaks of lower intensity as compared to those of ZnO. This UV emission peak confirms electron transition from a lower conduction band to the valence band. The population of Zn interstitial defects (Zn_i) is fairly sparse in the MgO/ZnO composite as shown by a small PL intensity (Fig. 4). For MgO/ZnO composites, the intensity of blue emission has increased due to the interstitial Mg (Mg_i) and Zn vacancy (Zn_v) recombination [19]. It can thus be suggested that within creasing MgO content, the concentration of surface defects in the MgO/ZnO composite increases until MgO content reached its optimum value. In addition, the recombination of an electron trapped in Zn_v could cause a rising to blue emission in MgO/ZnO composites. As a result, higher PL intensity and red shift from the exciton absorption peak reflects an increased population of crystallite defects in a certain material. Therefore, it seems that Mg_5Zn_5 composite has more surface defect sites than Mg_2Zn_5 and Mg_8Zn_5 composites, excellent photocatalytic activity of which can be clearly recognized on Figs 5 and 6.

Kinetic and Photocatalytic Experiments

The photocatalytic activity of MgO/ZnO composites was evaluated following the degradation of 2,6-DCP in a specially designed UV reactor. A 2,6-DCP stock solution (10 mg/L) was freshly prepared. Aliquots of 50 mL from this solution and 0.1 g of catalyst were transferred into the UV reactor and stirred for 60 min in dark to obtain adsorption-desorption equilibrium. After every 15 min, 1 mL of sample was withdrawn and filtered to monitor degradation rates. The degradation progress was monitored spectrophotometrically (Dr. Lange 1601 UV-vis) at $\lambda_{max} = 298$ nm. The degradation (%) of 2,6-DCP was calculated using the following equation:

$$\%\,\text{Degradation} = \frac{C_0 - C}{C_0} \times 100 = \frac{A_0 - A_t}{A_0}, \qquad (3)$$

where A_0 and A_t are the initial and final absorbencies of 2,6-DCP. According to the Beer–Lambert law, initial and final absorbencies correspond to the initial (C_0) and final (C) concentrations of 2,6-DCP [16].

Results obtained from photocatalytic activity are shown in Fig. 5. Pure ZnO exhibited lower photocatalytic activity (38%) due to either lower inhibition of e^--h^+ pairs or lower BET surface area. With increasing amount of MgO in ZnO photocatalytic activity

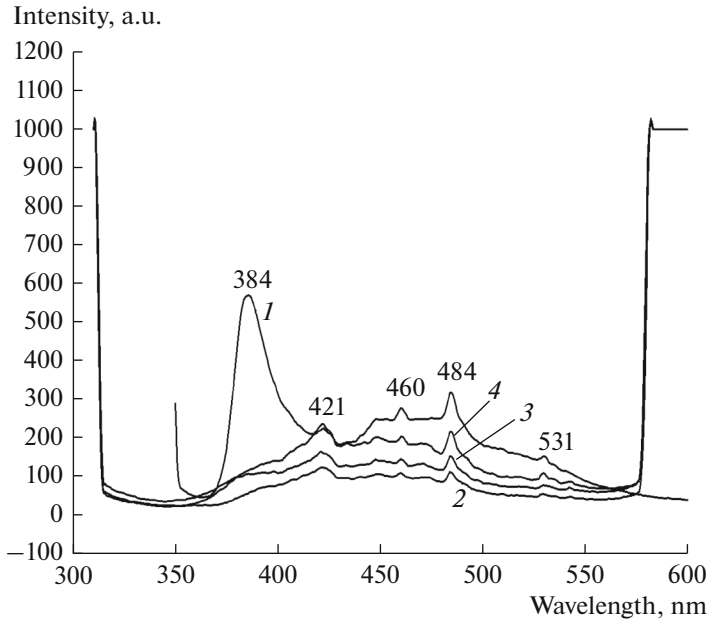

Fig. 4. PL spectra of ZnO (*1*) and MgO/ZnO composites: (*2*) Mg_2Zn_5, (*3*) Mg_8Zn_5, (*4*) Mg_5Zn_5.

increased. Within various MgO/ZnO composites Mg_5Zn_5 catalyst exhibited an efficient photoactivity (79.5%) in degradation of 2,6-DCP. Under the same conditions, the yield of degradation products was 63 and 61%, for Mg_2Zn_5 and Mg_8Zn_5, respectively. These results can be related to a larger specific surface area of Mg_2Zn_5 (74 m^2/g) compared to that of Mg_8Zn_5 (67 m^2/g). Thus, higher adsorption ability of 2,6-DCP on the composite surface provided efficient degradation (Table 1). Additionally, a higher degree of aggregation estimated for the Mg_8Zn_5 catalyst may have been a reason why its photocatalytic activity is lower than that shown by the Mg_2Zn_5 sample.

Mg_5Zn_5 catalyst showed a higher photocatalytic activity (79.5%) in the degradation of 2,6-DCP. Pseudo-first order kinetic equation can be used to explain the sequence of the photocatalytic reaction. First order kinetic rate k (min^{-1}) for 2,6-DCP degradation can be calculated by plotting $\ln\frac{C_0}{C}$ vs time (t) (Fig. 6). A higher rate constant means more efficient degradation (Table 1) [17]. Figure 7 shows UV-vis

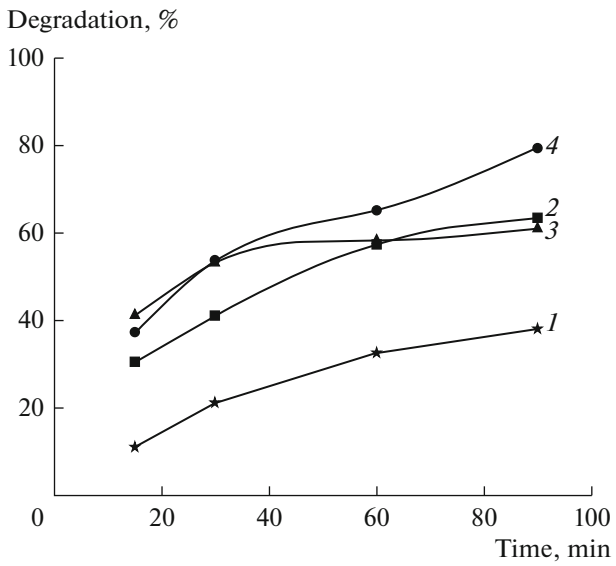

Fig. 5. Degradation kinetics of ZnO (*1*) and MgO/ZnO composites: (*2*) Mg_2Zn_5, (*3*) Mg_8Zn_5, (*4*) Mg_5Zn_5.

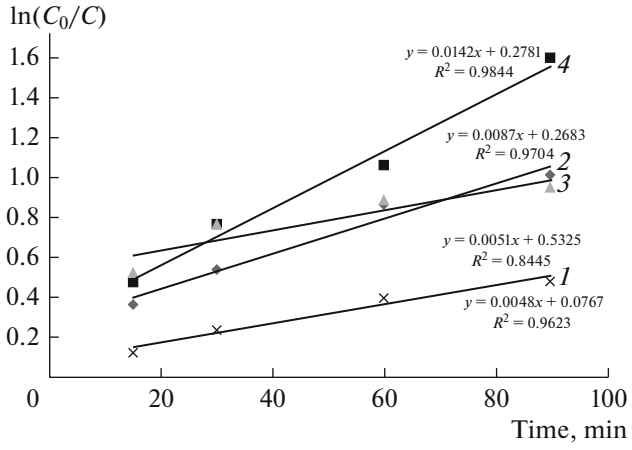

Fig. 6. Photocatalytic kinetics of ZnO (*1*) and the as-prepared MgO/ZnO composites: (*2*) Mg_2Zn_5, (*3*) Mg_8Zn_5, (*4*) Mg_5Zn_5.

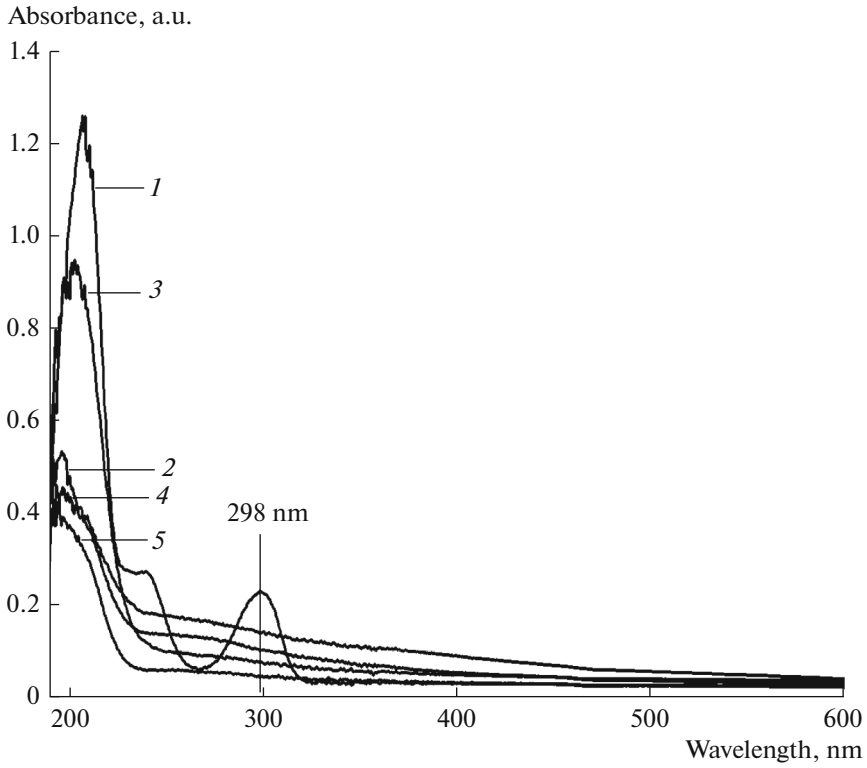

Fig. 7. UV-vis spectra of 2,6-DCP solutions using Mg_5Zn_5 catalyst at different degradation times, min: (*1*) 0, (*2*) 15, (*3*) 30, (*4*) 60, (*5*) 90.

spectra of 2,6-DCP decomposition registered at different time intervals. After 90 min, there is a remarkable decrease in the absorbance that confirms the effective decomposition of 2,6-DCP in the presence of the Mg_5Zn_5 catalyst.

Interestingly, the BET surface area of Mg_5Zn_5 was found to be smaller (57 m^2/g) than that of Mg_2Zn_5 and Mg_8Zn_5 composites. It can be assumed that positive results obtained from the photocatalytic activity of Mg_5Zn_5 catalyst are not due to the surface area of the catalysts. The band gap value of MgO was estimated to be higher than that of ZnO. In other words, the conduction and valence band values are between the MgO band offsets (Fig. 8) [18]. The photocatalytic performance of Mg_5Zn_5 can be associated with the crystallite defects as explained by the following argumentation.

(i) The 2,6-DCP molecules adsorbed on the catalyst surface and also the electrons in the valence band (VB) of ZnO were excited to its defect level, which exhibited extra holes (h^+) in the ZnO and conduction band (CB) level. The oxygen vacancies (V_0) that lie below the composite surface can capture a hole (h^+) in the defect level to be transformed into (V_0^+) species [13]. This V_0^+ species could catch an electron to form oxygen vacancy (O_v).

(ii) The photoexcited electrons in the defect level of ZnO can also be transferred to its CB to form superox-

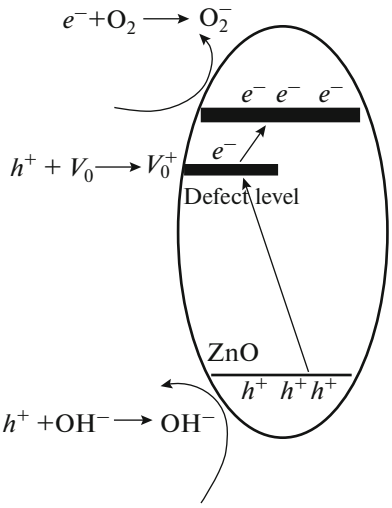

Fig. 8. Schematic illustration of photocatalytic mechanism of Mg_5Zn_5 composite.

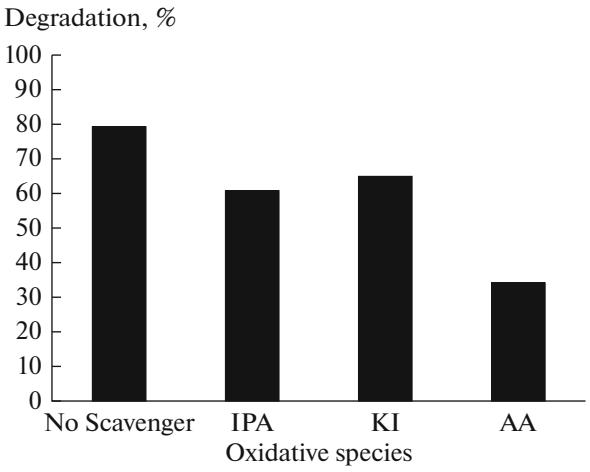

Fig. 9. Effects of different scavengers on degradation of 2,6-DCP in the presence of Mg_5Zn_5 composite photocatalyst.

ide radicals. Additionally, the photogenerated holes in the VB level of ZnO are able to produce hydroxide radicals, which decompose 2,6-DCP molecules.

(iii) The migrating electrons of ZnO in the defect level and its CB electrons can generate superoxide $\left(O_2^{\bullet-}\right)$ radicals and photogenerated holes in the VB level of ZnO to produce hydroxide $\left(OH^{\bullet}\right)$ radicals by reacting with O_2 and hydroxide, respectively.

The inhibition of the recombination rate of electron-hole pairs results in an efficient degradation in the presence of the Mg_5Zn_5 catalyst (Fig. 8). Also, the E_g values of each composite are slightly different. These results indicate that the band gap is hardly a primary factor that affects the photocatalytic performance of MgO/ZnO composites in the degradation of 2,6-DCP.

Photocatalytic Mechanism

It is well known that active oxidizing species i.e. $\left(O_2^{\bullet-}\right)\left(h^+\right)\left(OH^{\bullet}\right)$ appears during the light irradiation and that they are responsible for the degradation of dye molecules under study. The photoexcited electrons and the adsorbed O_2 on the catalyst surface produce superoxide $\left(O_2^{\bullet-}\right)$ radicals and the photogenerated holes, while water is the source of hydroxyl radicals $\left(OH^{\bullet}\right)$. Isopropanol (IPA), potassium iodide (KI) and ascorbic acid (AA) are used as scavengers to explain the catalytic mechanism for MgO/ZnO composites [19]. Figure 9 shows the degradation of 2,6-DCP in the presence of scavengers. The degree of degradat ion decreased from 79.5% (no scavenger) to 65 and 61% when 1 mmol/L of IPA and KI were used, respectively. These results reveal that $OH^{\bullet}$ radical plays a minor role in the degradation of 2,6-DCP. To study the role of $\left(O_2^{\bullet-}\right)$ radical, ascorbic acid (1 mmol/L) was used as a superoxide scavenger [20]. A significant decrease (to 34.5%) in the photodegradation of 2,6-DCP could then be observed (Fig. 8). It can be thus inferred that the superoxide radical $\left(O_2^{\bullet-}\right)$ plays a major role while the contribution of $OH^{\bullet}$ in the photodegradation of 2,6-DCP is less significant. The use of superoxide radical $\left(O_2^{\bullet-}\right)$ markedly inhibited the photocatalytic activity of Mg_5Zn_5 (Fig. 9).

HRMS Analyses

Initial 2,6-DCP (m/z = 163, Fig. 10a) and 2,6-DCP subjected to photodegradation for 90 min (Fig. 10b) were analyzed by HRMS. The spectrum (b) showed peaks at m/z = 163.2315 and 168.0448 implying that 2,6-DCP was not transformed into hydroquinone in the presence of MgO/ZnO composites. Figure 10b shows that 2,6-DCP was successfully decomposed to lower bi-products with m/z of 82.0175, 110.0310 and 124.0908 as summarized in Table 2.

Table 2. Proposed degradation byproducts of 2,6-DCP

m/z	Proposed possible molecules [M – H]
163.1258 (2,6-DCP)	$C_6H_4Cl_2OH$
124.0908 and closer values	C_6H_4ClOH
110.0310 and closer values	C_6H_4Cl (m/z = 110.01), and opening benzene ring $C_4H_4O_4$ (m/z = 115.02), $C_3O_4H_3$ (m/z = 110.02), C_2O_2ClH (m/z = 90.98)
82.0175 and closer values	$CClO_2H$ and opening benzene ring

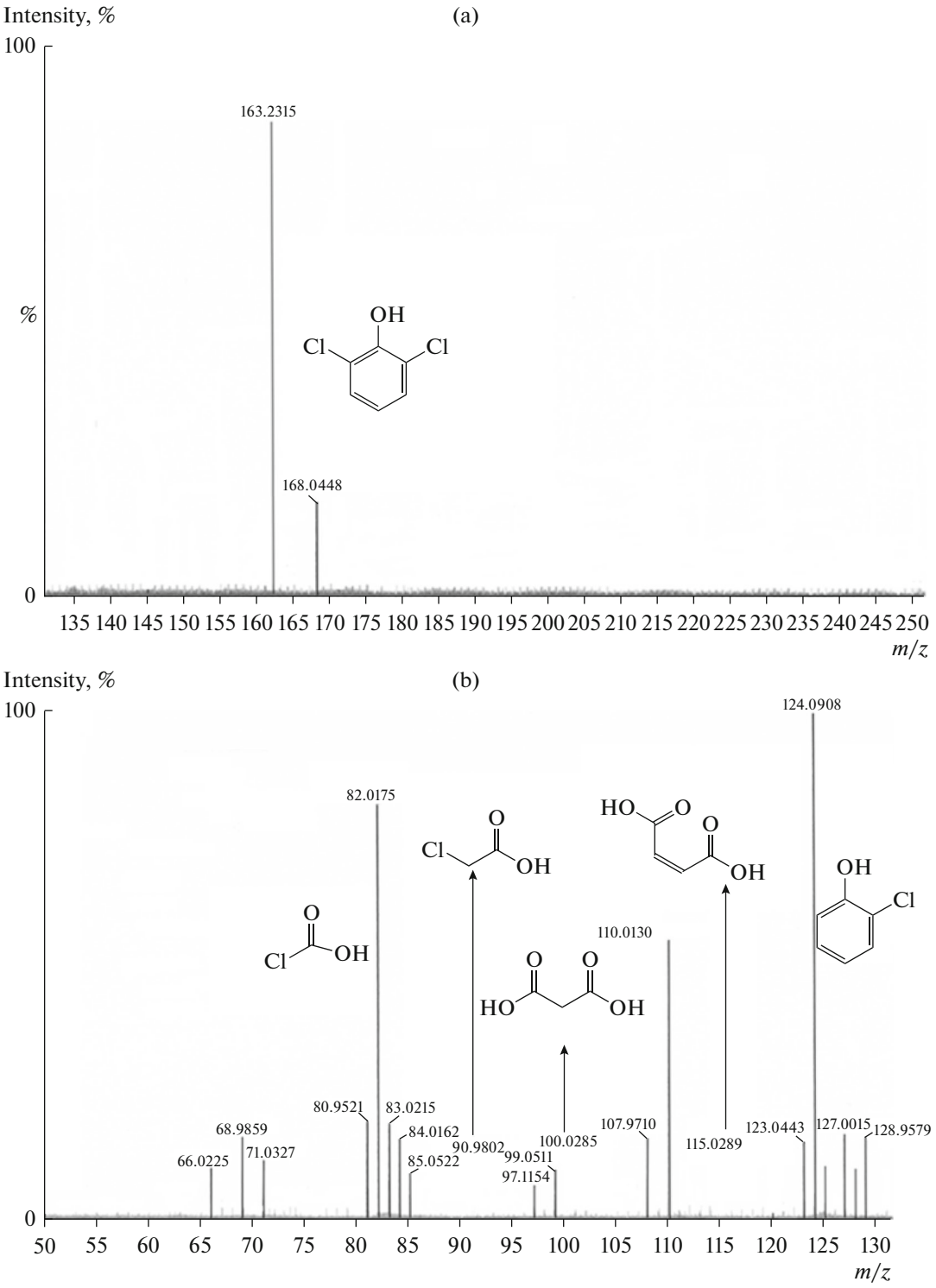

Fig. 10. HRMS results of 2,6-DCP (in the presence of Mg_5Zn_5 catalyst) (a) and after 90 min contact (b).

CONCLUSIONS

MgO/ZnO composites were synthesized by a co-precipitation method using $Mg(NO_3) \cdot 2H_2O$ and $Zn(Ac)_2 \cdot 6H_2O$. Each sample was calcined at 600°C for 3 h. MgO content affected the catalytic and optical properties of ZnO in different ways. SEM images show that all samples were nearly spherical while their morphology was unchanged after MgO loading. The E_g value of pure ZnO (3.44 eV) was lower than that of MgO/ZnO composites because the ZnO structure contained an enhanced concentration of defect sites.

Mg_5Zn_5 composite with a higher concentration of defects in crystallites was more active in the photocatalytic degradation (79.5%) than Mg_8Zn_5 (61.2%) and Mg_2Zn_5 (63.5%).

ACKNOWLEDGMENTS

This manuscript is supported by the Mugla Sitki Kocman University coordination of scientific research projects (BAP) 15/139.

REFERENCES

1. Beydoun, D., Amal, R., Low, G., and McEvoy, S., *J. Nanopart. Res.*, 1999, vol. 1, p. 439.
2. Zhao, X., Li, M., and Lou, X., *Adv. Powder Technol.*, 2014, vol. 25, p. 372.
3. Suwanboon, S., Klubnuan, S., Jantha, N., Amornpitoksuk, P., and Bangrak, P., *Mater. Lett.*, 2014, vol. 115, p. 275.
4. Vaizogullar, A.I., *Theor. Exp. Chem.,* 2017, vol. 53, p. 31.
5. Klubnuan, S., Amornpitoksuk, P., and Suwanboon S., *Mater. Sci. Semicond. Process.*, 2015, vol. 39, p. 515.
6. Zhao, J., Mu, F., Qin L., Jia, X., and Yang, C., *Mater. Chem. Phys.*, 2015, vol. 166, p. 176.
7. Al-Naser, Q.A.H., Zhou, J., Wang, H., Liu, G., and Wang, L., *Opt. Mater.*, 2015, vol. 46, p. 22.
8. Babu, K.S., Reddy, A.R., and Reddy, K.V., *J. Lumin.*, 2015, vol. 158, p. 306.
9. Suwanboon, S., Amornpitoksuk, P., Bangrak, P., and Muensitd, N., *Ceram. Int.*, 2013, vol. 39, p. 5597.
10. Ohtani, B., *J. Photochem. Photobiol., C.*, 2010, vol. 11, p. 157.
11. Senger, R. and Bajaj, K., *Phys. Rev. B*, 2003, vol. 68, p. 1.
12. Kim, H.W., Shim, S.H., and Lee, C., *Mater. Sci. Eng. B*, 2007, vol. 136, p. 148.
13. Tabib, A., Bouslama, W., Sieber, B., Addad, A., Elhouichet, H., Ferid, M., and Boukherrou, R., *App. Surf. Sci.*, 2017, vol. 396, p. 1528.
14. Belaissa, Y., Nibou, D., Assadi, A.A., Bellal, C., and Trari, M., *J. Taiwan Inst. Chem. Eng.,* 2016, vol. 68, p. 254.
15. Singh, D.P., Singh, J., Mishra, P.R., Tiwari, R.S., and Srivastava, O.N., *Bull. Mater. Sci.*, 2008, vol. 31, no. 3, p. 319.
16. Suwanboon, P., Amornpitoksuk, S., and Muensit, J., *J. Ceram. Process. Res.*, 2010, vol. 11, p. 419.
17. Lyu, S.C., Zhang, Y., Ruh, H., Lee, H.J., Shim, H.W., Suh, E.K., and Lee, C.J., *Chem. Phys. Lett.*, 2002, vol. 363, no. 1, p. 134.
18. Umar, A., Choi, Y.J., Suh, E.K., Al-Hajry, A., and Hahn, Y.B., *Curr. Appl. Phys.*, 2008, vol. 8, no. 6, p. 798.
19. Shirzadi, A. and Ejhieha, A.N., *J. Mol. Catal. A.: Chem.*, 2016, vol. 411, p. 222.
20. Ye, J., Li, X., Hong, J., Chen, J., and Fan, Q., *Mater. Sci. Semicond. Process.*, 2015, vol. 39, p. 17.